



Offshore COVID-19 risk assessment based on a fishing vessel

Luofeng Huang^{a,*}, Wolter Hetharia^b, Andrea Grech La Rosa^c, Sasan Tavakoli^d,
Danial Khojasteh^e, Minghao Li^f, Soengeng Riyadi^g, Dony Setyawan^g, I.K.A.P. Utama^g,
Giles Thomas^c

^a School of Water, Energy and Environment, Cranfield University, Cranfield, UK

^b Department of Naval Architecture, University of Pattimura, Ambon, Indonesia

^c Department of Mechanical Engineering, University College London, London, UK

^d Department of Infrastructure Engineering, The University of Melbourne, Melbourne, Australia

^e School of Civil and Environmental Engineering, University of New South Wales, Sydney, Australia

^f Department of Mechanics and Maritime Sciences, Chalmers University of Technology, Gothenburg, Sweden

^g Department of Naval Architecture, Institut Teknologi Sepuluh Nopember, Surabaya, Indonesia

ARTICLE INFO

Keywords:

Pandemic
Offshore operation
Fishing vessel
Virus
Risk assessment
Computational fluid dynamics
Particle modelling
Particulate flow

ABSTRACT

Offshore crews often work near each other due to limited space, signifying a complex environment for the airborne transmission of the coronavirus (COVID-19). During offshore operations, a fishing vessel can be subjected to miscellaneous airflow conditions and will respond dynamically to ocean waves. To understand the risk of COVID-19 contagion, this research establishes a new computational model to analyse the airborne transmission of COVID-19 and develops effective mitigation strategies where possible. The concentration and coverage of coronavirus are scrutinised, considering typical airflows and wave-induced vessel motions. Furthermore, the COVID-19 infection risk is quantified using a probability index. The results show that the overall infection risk of a ship in tailwind is lower than in head or beam wind. Structural motions are for the first time coupled with the virus transmission, and it was found that the vessel's oscillating movement in waves can reinforce the virus concentration in close proximity to the infected person and may help diffuse the virus outside the proximal region. The presented findings can inform the airborne contagion risks and corresponding hygienic measures for maritime and offshore operations, facilitating long-term human health in seas.

1. Introduction

COVID-19 is one of the world's largest crises and has posed pervasive threats to different sectors of society and the environment (Khojasteh et al., 2022). In particular, it has severely debilitated the offshore and maritime industry since workers and passengers are normally required to be in close proximity, especially when there is limited space (Chua et al., 2022). Since the commencement of the COVID-19 outbreak, a number of incidents of coronavirus outbreaks were reported on cruise ships around the world (Almilaji, 2021; Azimi et al., 2021). Being aware of the high contagion risk at sea, countries had intermittently suspended ship operations and offshore projects over pandemic peaks, or imposed social distancing and quarantine regulations such that ships had to operate at a significantly reduced capacity (Thomas et al., 2021). Even though most countries have recently loosened COVID-19 restrictions, there is still a risk of more COVID-19 case surges due to virus variants

(Zhao et al., 2022). In the meantime, offshore and maritime sectors are still suffering from the negative impact of COVID-19 including poor morale and increased operational costs compared to the pre-pandemic level (Tu et al., 2021; D'Antoine et al., 2023).

To enhance the economic recovery in the industry and inform public health regulations, scientific research is required to ensure the rationality of relevant operational guidelines and rebuild workers' confidence. In this context, it is essential to investigate the virus transmission mechanism as well as the infection risks in different scenarios. The COVID-19 transmission mechanism has been relatively well understood where viruses are primarily spread via air and through aerosols and droplets originated from the mouth and nose of an infected person (Wang et al., 2021). The aerosol and droplet particles may float in the air for a period of time before sinking to the ground. They are driven by airflow to travel and diffuse, where the diffusion dictates the virus concentration and coverage (Vuorinen et al., 2020; Ando et al., 2022).

* Corresponding author.

E-mail address: luofeng.huang@cranfield.ac.uk (L. Huang).

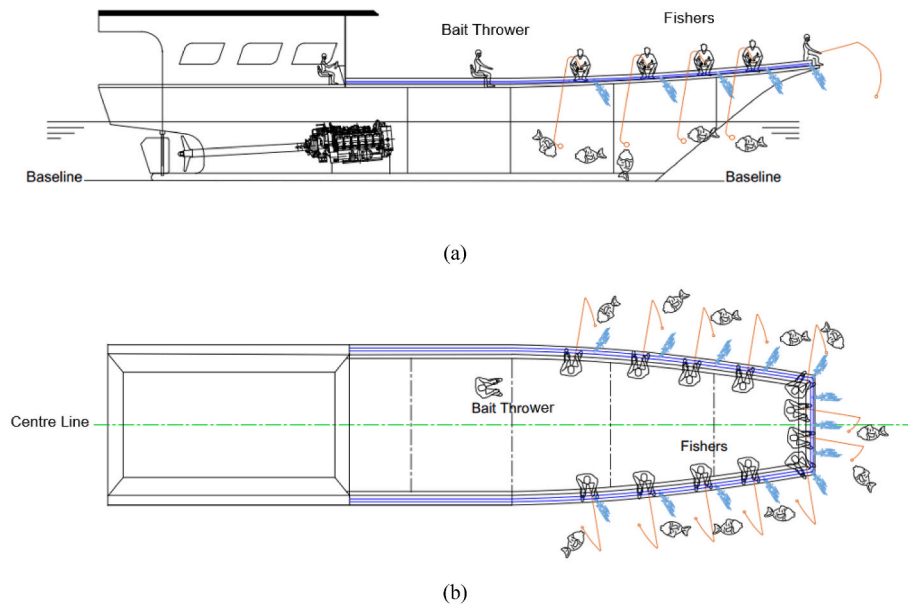


Fig. 1. Schematic of the PL fishing method: (a) Profile view, (b) Plan view.

Therefore, a key step in understanding and mitigating the COVID-19 risk is to accurately assess and predict the virus concentration and coverage in typical scenarios.

Computational Fluid Dynamics (CFD) has become a standard approach for studying COVID-19 airborne transmission phenomena. This method has been widely applied for the replication of complex airflows and tracking the trace of virus particles through a Lagrangian approach. Vuorinen et al. (2020) were one of the earliest that used CFD to show the virus concentration and trace following an infected person's cough, alongside how this interacts with an in-door ventilation system. Huang et al. (2022a) developed a CFD model for predicting the virus transmission inside the superstructure of a passenger ship and used experimental data to validate the model. The comparison showed that the model predicts virus velocity and concentration profiles with high accuracy. They suggested a series of mitigation measures such as social distancing and controlling air conditioner flows. Zhang et al. (2021) compared experimental and CFD studies to provide an understanding of the transmission of COVID-19 on a bus, where they demonstrated the CFD approach can reasonably simulate the virus trace. Similar comparative studies between experiments and CFD models for COVID-19 spreading events have been given by Jeong et al. (2022) and Janoszek et al. (2021). Sarhan et al. (2021) used simulations to highlight that social distancing in indoor environments may not be effective when the virus transmission is governed by airflow. Thanigaiarasu et al. (2022) developed a function indicating that increasing airflow velocity corresponds to decreasing the total travelable distance of coronavirus aerosol and droplet particles before sinking to the floor. The simulations performed by Abugazy et al. (Abuhegazy et al., 2020) and Talaat et al. (2021) confirmed that using lateral shields between people can reduce COVID-19 transmission risk in confined spaces. Zhang et al. (2022) used CFD to demonstrate the spread of COVID-19 in a grocery store highlighting that ventilation can create some accumulated viruses near walls and corners, as also reported by Huang et al. (2022a). While governments occasionally banned mass gatherings due to the perceived rise in COVID-19 transmission, Moritz et al. (2021) used a CFD model to indicate that there is no such effect as long as standard ventilation is applied. This finding was later corroborated by the physical measurements conducted by Adzic et al. (2022). Bale et al. (2022) demonstrated that CFD can further be used to quantify COVID-19 risks based on the predicted virus concentration. Using such a quantitative risk index, Wang et al. (2022) simulated the virus transmission inside a train and

reported the infection probabilities of different seat locations. Overall, CFD has significantly enhanced the understanding of COVID-19 transmission, and helped to inform global protocols and guidelines, including social distancing, masks/shields, disinfection systems, and ventilation controls (Ando et al., 2022; Mohamadi and Fazeli, 2022).

Despite the aforementioned contribution of CFD in COVID-19 research, this approach has scarcely been applied to offshore scenarios. Recently, Tavakoli et al. (2023) presented a horizon scanning of literature related to ocean engineering, explicitly indicating that COVID-19 research for offshore environments is absent, except for Huang et al. (2022a). Offshore outbreak scenarios for airborne virus transmission are unique. For example, ships can have a door at the front of the cabin area which is different from cars, trains or aeroplanes. When the ship is underway, the forward door may be opened to allow a significant wind flow to enter the passengers' area and drive the virus spread, as studied by Huang et al. (2022a).

Another typical scenario in offshore environments, that has not been studied for its COVID-19 risk, is the transmission on an open-air deck or platform. For instance, the Pole & Line (PL) fishing process, as shown in Fig. 1, typically requires 10 or more crew members working side-by-side to angle fish out of the sea. The physical demands of this type of fishing make it difficult to wear face masks since they might cause breathing difficulty during such moderate impact cardio activities. The ship is also subjected to various airflows as well as heave, pitch, and roll motions due to the oceanic waves, creating complex patterns of virus transmission. Under these circumstances, the crew's COVID-19 safety is of concern.

In this context, this research develops a CFD-based model to analyse the potential transmission of COVID-19 on a PL fishing vessel. This is for the first time that COVID-19 is studied in an open-air offshore environment, and a novel computational approach is introduced that demonstrates the coupling of the airborne virus transmission with a moving carrier, e.g. an oscillating ship in waves. The present paper first presents the case and the corresponding model in detail. The model is then used to predict the virus spread and distribution in different scenarios concerning varying wind speeds/directions as well as vessel motions. Finally, a risk assessment approach is applied to quantitatively discuss the risks and mitigative strategies. The conclusions from this study can help minimise the offshore transmission of COVID-19 or any other similar viruses.



Fig. 2. The fishing vessel used in this study, named “Yora 02”

Table 1
Dimensions (in meters) of the ship model in this study.

Overall length	18.85
Waterline length	16.20
Overall Beam	4.20
Waterline beam	3.30
Depth	3.06
Draught	1.05
Deck height	2.01
Vertical centre of gravity from keel	1.5
Longitudinal centre of gravity from aft perpendicular	7.0

2. Computational approach

2.1. Ship model and computational domain

A standard PL fishing vessel operating in Indonesia was selected as the case study for this paper, as depicted in Figs. 1 and 2. The fishing

industry is particularly important for Indonesia where there are approximately 2.2 million fishers and 600,000 fishing vessels (Wibawa and Birmingham, 2018). The ship selected has the following dimensions: overall length = 18.85 m, beam = 4.2 m, and draught = 1.05 m, with more details presented in Table 1. Based on a common PL working setup, it is assumed that 13 fishers are working in the bow area, in which, 5 crew are in the bow and 4 crew are on the port or starboard side. In addition to this, one bait thrower works from the deck’s centreline. Typically, there is a distance of 0.5 m between two adjacent fishermen (head-to-head distance). Based on the above case, the computational geometry of the ship and fishers was built at a full scale, as illustrated in Fig. 3.

To perform CFD investigations, the vessel and fisher geometry was imported into the STAR-CCM + software. A rectangular computational domain was then established (60 m × 60 m × 30 m), with the ship located at its centre with a water depth of 15 m. The domain size meets the CFD standard that it is large enough to model an open-ocean environment, i.e. no reflective flows from any boundary can interact with the

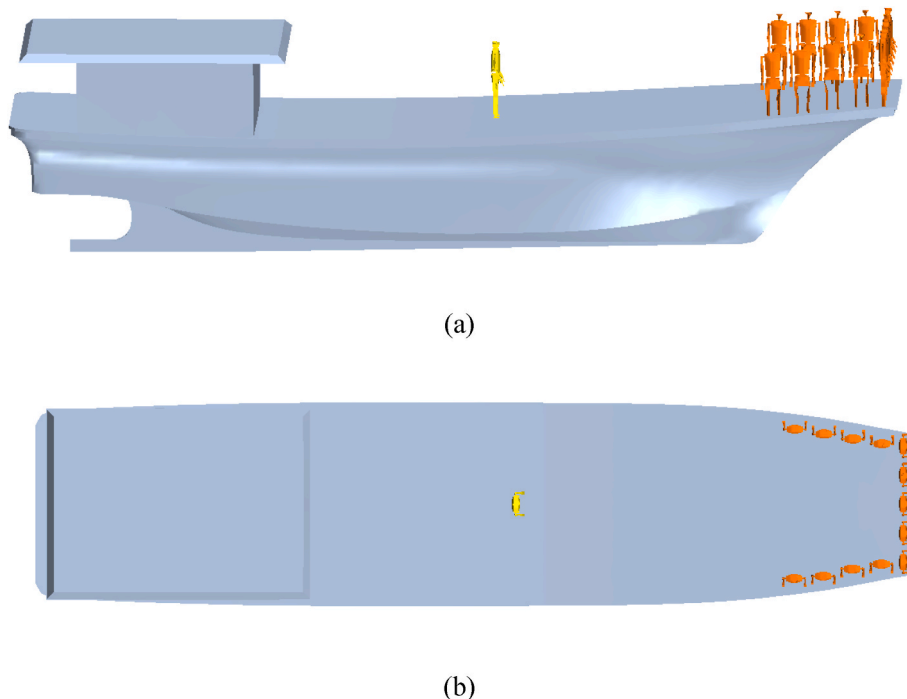


Fig. 3. Computational geometry of the ship and crew, with fishers coloured orange and the bait thrower coloured yellow: (a) Profile view, (b) Plan view.

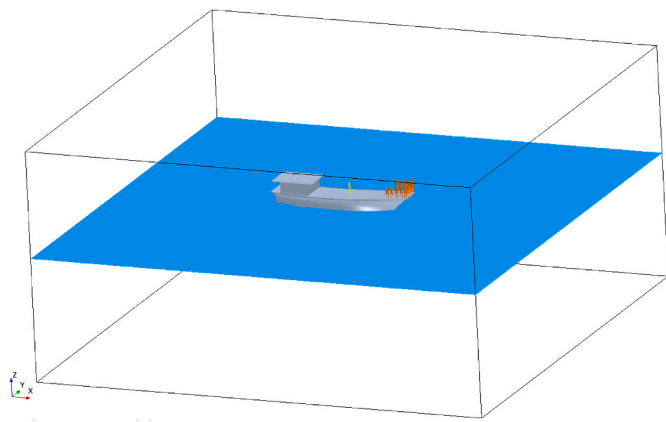


Fig. 4. Computational domain, free surface and the geometries.

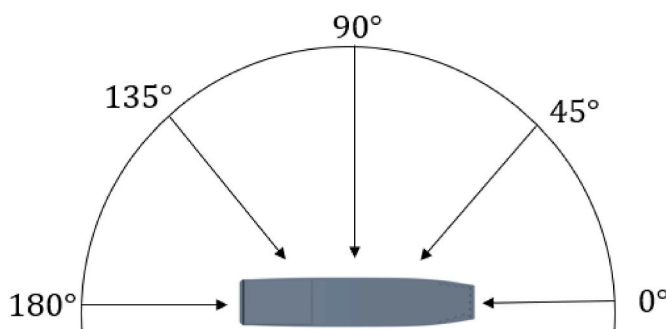


Fig. 5. Incoming airflow directions (θ) simulated in this study.

Table 2
The details of virus import due to speaking (Chao et al., 2009).

Speed of injected particles	3.1 m/s
Particle diameter	16 μm
Injected particle number	443 per second

ship (ITTC, 2014; Huang et al., 2023). A free surface was inserted according to the waterline of the ship. Fig. 4 shows the generated computational domain and free surface.

The ship was assumed to operate in airflows from different directions and at varying velocities. Five directions of airflows were studied, namely $\theta = 0^\circ, 45^\circ, 90^\circ, 135^\circ,$ and 180° , where $\theta = 0^\circ$ denotes a head wind as indicated in Fig. 5. These directions are complemented with five

different relative airflow velocities of $V = 1, 2, 3, 4,$ and 5 m/s, producing 25 simulation cases. Simulations considering ship motions in waves were compared to the calm water equivalent.

The boundary conditions to simulate the ship in various airflows are described as follows. The boundary from which the air comes is set as the “inlet” with a constant airflow velocity of $(V, 0, 0)$ m/s. The opposite boundary to the inlet is set as the “outlet” with a fixed reference pressure of 0 Pa; This value is insignificant since the CFD calculation is based on relative pressure. The ship surface is set at “non-slip walls” with a fixed velocity of $(0, 0, 0)$ m/s. In this manner, there is a relative speed $(V, 0, 0)$ between the ship and the airflow. The airflow coming from different directions is simulated by rotating the domain by θ whilst remains the ship in the same direction.

2.2. Virus injection

The source of COVID-19 virus in this work is considered to be an infected person speaking on board. Airborne COVID-19 exists in the forms of aerosols and droplets that can be generated by humans coughing, speaking, breathing, singing, and sneezing (Wang et al., 2021). Coughing and speaking are the most likely scenarios, as coughing is one of the primary COVID-19 symptoms whilst speaking is almost inevitable in daily contact and can output a significant virus particle count. Chao et al. (2009) measured the velocity, concentration and diameter of virus particles from coughing and speaking. They suggested that the duration of coughing is around 0.3 s, whilst speaking was considered to last 60 s. The viruses injected through coughing have a higher concentration and initial speed than those from speaking. However, the total quantity of viruses injected from speaking can be more than coughing as its duration is much longer, thus a higher possibility for a healthy person to inhale sufficient viruses that causes infection (Huang et al., 2022a). Therefore, the present study considered speaking over coughing as the source of virus generation. The injection location of the virus into the computational domain is assumed to be the infected person’s mouth. The injection is continuous with a given amount of particles per second, and the injected particle has an initial speed following the nature of speaking. Table 2 gives the magnitudes of the injected particle’s initial speed, the particle diameter, and injected particle number per second, where the values are from the physical measurements of Chao et al. (2009)Chao et al. (. For different simulation cases with different wind directions, the upstream person is selected as the infected one, which is to ensure the maximal risk is studied. An example of injected viruses and their diffusion is illustrated in Fig. 6.

2.3. Governing equations

The COVID-19 aerosols/droplets were modelled as Lagrangian par-

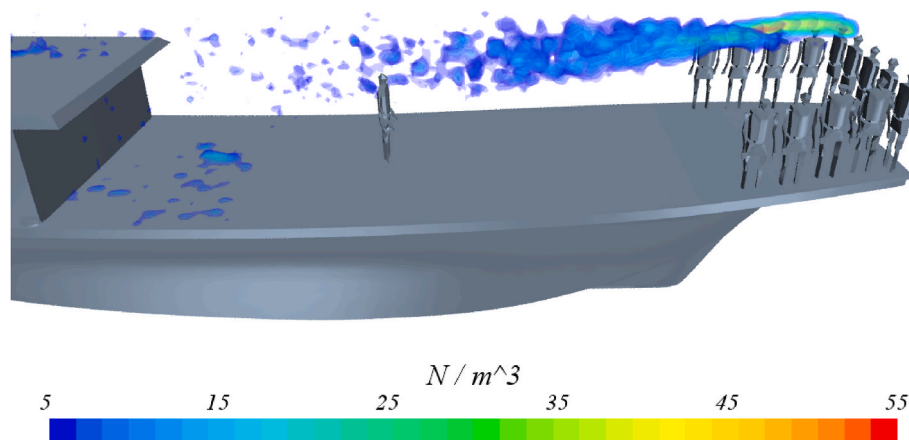


Fig. 6. Example of and their diffusion in airflow. $V = 2$ m/s, $\theta = 0^\circ$, and N/m^3 stands for particle number per cubic meter.

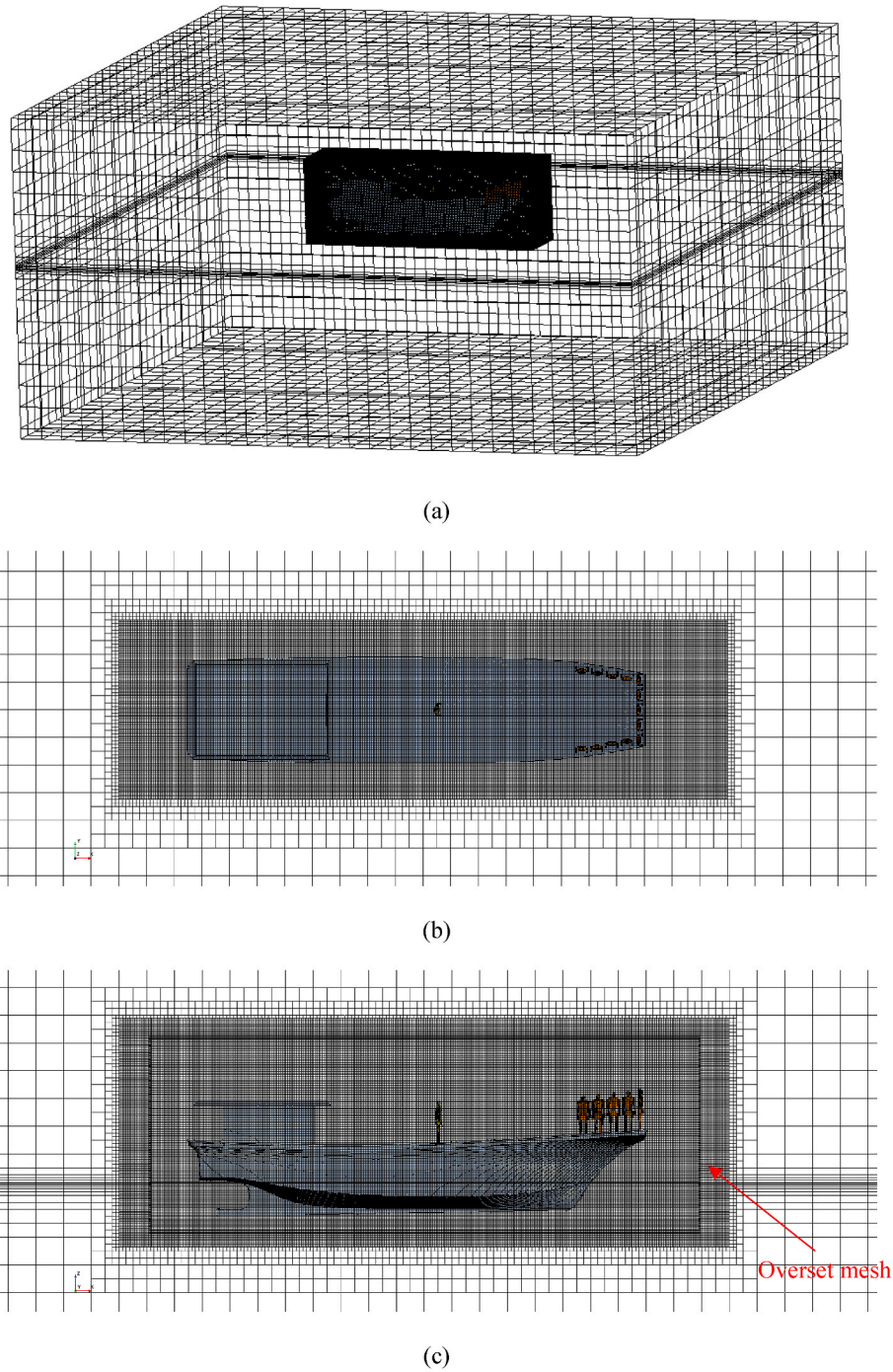


Fig. 7. Discretised computational domain with local refinements applied to overset and free surface regions: (a) Whole domain, (b) Plan view close-up, (c) Profile view close-up.

ticles, and the particle shape is spherical. The particles were allowed to freely move in the Eulerian fluid domain, through a one-way coupling approach, i.e. the particles gain momentum from the fluid flow while the particle movement does not influence the flow velocity or pressure. The one-way mechanism is reasonable as the COVID-19 particle size is too small to alter the flow. The particles' movement is determined by their gravity (G) and a drag force resulting from the surrounding airflow (F_d) as expressed in Equation (1)

$$m \frac{d\overline{V}_p}{dt} = G + F_d \quad (1)$$

where m denotes the particle's mass, \overline{V}_p is the particle's velocity, and G

$= mg$ with g is set at 9.81 m/s^2 . The fluid drag force is calculated using the Schiller-Naumann Correlation shown in Equation (2) (Liu et al., 1993):

$$F_d = \frac{1}{2} C_d \rho_p A_p |V_s| V_s \quad (2)$$

where ρ_p is the particle density, A_p is the particle projected area, and V_s is the relative velocity between the particle and the air. C_d is an empirical drag coefficient calculated based on the particle's Reynolds number (Re_p), which is defined as shown in Equation (3).

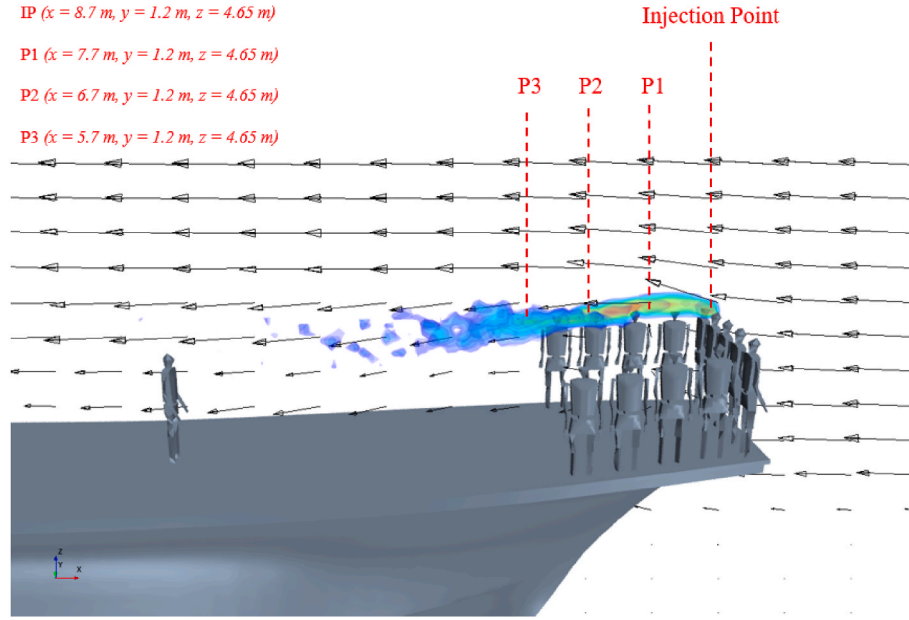


Fig. 8. Locations of data points for the mesh sensitivity study - Injection Points (IP), Point 1 (P1), Point 2 (P2), Point 3 (P3).

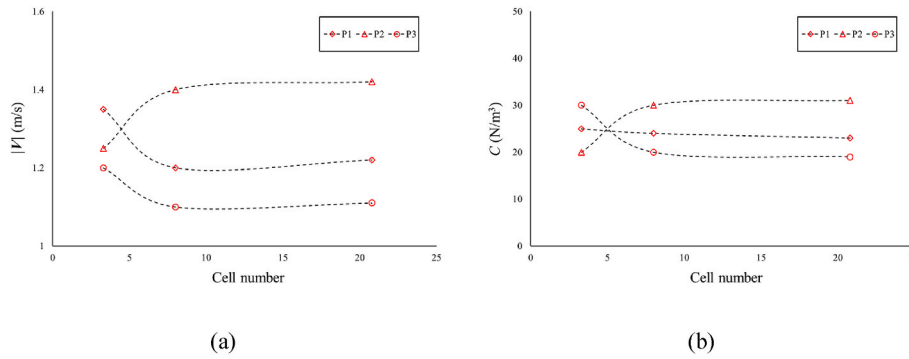


Fig. 9. Results of the mesh sensitivity study: (a) Velocity Magnitude ($|V|$), (b) Particle concentration (C).

$$C_d = \begin{cases} \frac{24}{Re_p} (1 + 0.15 Re_p^{0.687}), & \text{if } Re_p \leq 1000 \\ 0.44, & \text{if } Re_p > 1000 \end{cases} \quad (3)$$

Fluid flow characteristics in the CFD mesh were obtained by solving the standard Reynolds-Averaged Navier-Stokes (RANS) equations as shown in Equations (4) and (5):

$$\nabla \cdot \bar{\mathbf{v}} = 0 \quad (4)$$

$$\frac{\partial(\rho \bar{\mathbf{v}})}{\partial t} + \nabla \cdot (\rho \bar{\mathbf{v}} \bar{\mathbf{v}}) = -\nabla \bar{p} + \nabla \cdot (\bar{\boldsymbol{\tau}} - \rho \overline{\mathbf{v}' \mathbf{v}'} + \rho \mathbf{g}) \quad (5)$$

where $\bar{\mathbf{v}}$ is the time-averaged velocity, \mathbf{v}' is the velocity fluctuation, ρ is the fluid density, \bar{p} denotes the time-averaged pressure, $\bar{\boldsymbol{\tau}} = \mu[\nabla \bar{\mathbf{v}} + (\nabla \bar{\mathbf{v}})^T]$ is the viscous stress term, and μ is the dynamic viscosity. Since the RANS equations have been used to model fluid turbulence, the Shear Stress Transport (SST) $k - \omega$ model was adopted to close the equations (Menter, 1993; Pena and Huang, 2021).

COVID-19 particles are microscopic and can constantly perform stochastic motions. On a macro level, the stochastic motions are revealed as the particles gradually diffuse. This behaviour is modelled by including the effect of instantaneous velocity fluctuations on the particles as shown in Equation (6) (Gosman and Loannides, 1983):

$$\mathbf{v} = \bar{\mathbf{v}} + \mathbf{v}' \quad (6)$$

To be more specific, the applied fluid velocity in calculations is \mathbf{v} , which is different from a usual RANS approach for macroscopic problems where $\bar{\mathbf{v}}$ is directly used for simplification, e.g. (Huang et al., 2020).

The free surface between the air and water was modelled by the Volume of Fluid (VOF) method (Hirt and Nichols, 1981). The VOF method introduces a passive scalar α , denoting the fractional volume of a cell occupied by a specific phase. In this case, a value of $\alpha = 1$ corresponds to a cell full of water and a value of $\alpha = 0$ indicates a cell full of air. Thus, the free surface, which is a mix of air-water phases, is formed by the cells with $0 \leq \alpha \leq 1$. The transient elevation of the free surface is obtained by the advection equation of α , expressed as Equation (7). For a cell containing both air and water, the density and viscosity are determined by a linear average according to Equation (8) and Equation (9). In this study, $\rho_{\text{water}} = 998.8 \text{ kg/m}^3$, $\mu_{\text{water}} = 8.90 \times 10^{-4} \text{ N s/m}^2$, $\rho_{\text{air}} = 1 \text{ kg/m}^3$, $\mu_{\text{air}} = 1.48 \times 10^{-5} \text{ N s/m}^2$.

$$\frac{\partial \alpha}{\partial t} + \nabla \cdot (\bar{\mathbf{v}} \alpha) = 0 \quad (7)$$

$$\alpha = \alpha \rho_{\text{water}} + (1 - \alpha) \rho_{\text{air}} \quad (8)$$

$$\mu = \alpha \mu_{\text{water}} + (1 - \alpha) \mu_{\text{air}} \quad (9)$$

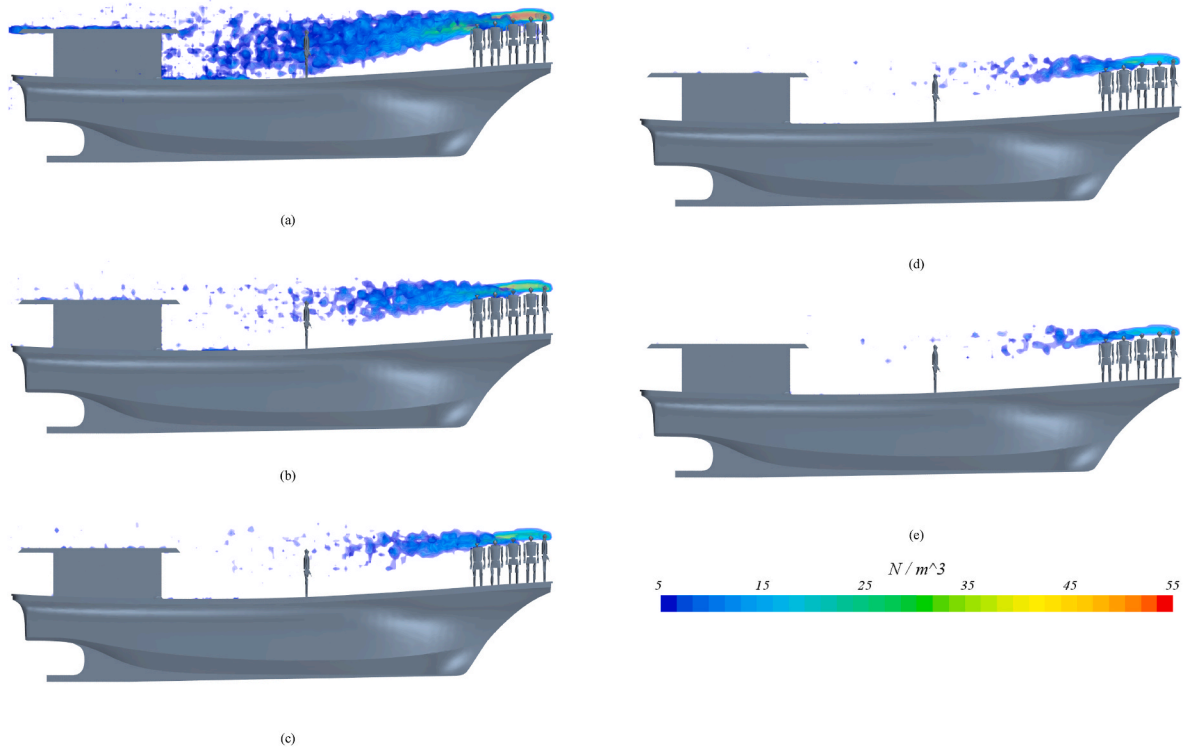


Fig. 10. Comparison of virus distribution with different wind speeds; profile view and $\theta = 0^\circ$: (a) $V = 1$ m/s, (b) $V = 2$ m/s, (c) $V = 3$ m/s, (d) $V = 4$ m/s, (e) $V = 5$ m/s.

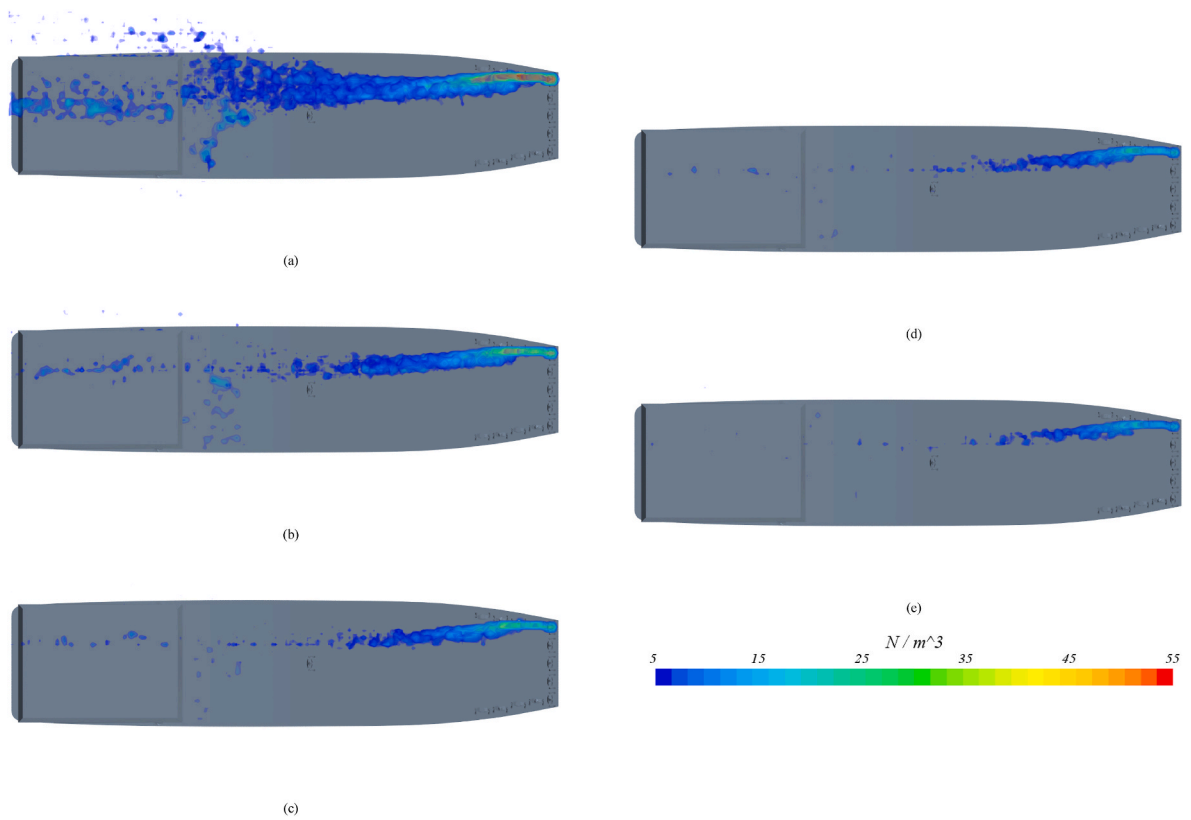


Fig. 11. Comparison of virus distribution with different wind speeds (V); plan view and $\theta = 0^\circ$: (a) $V = 1$ m/s, (b) $V = 2$ m/s, (c) $V = 3$ m/s, (d) $V = 4$ m/s, (e) $V = 5$ m/s.

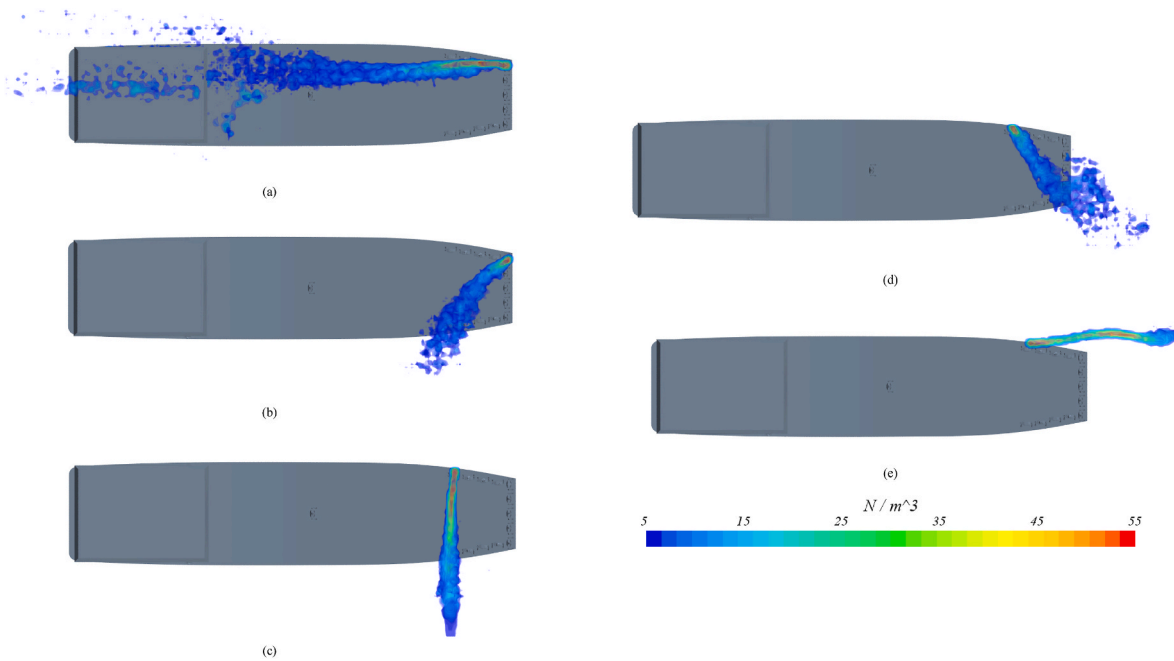


Fig. 12. Comparison of virus distribution with different wind directions; plan view and $V = 1$ m/s: (a) $\theta = 0^\circ$, (b) $\theta = 45^\circ$, (c) $\theta = 90^\circ$, (d) $\theta = 135^\circ$, (e) $\theta = 180^\circ$.

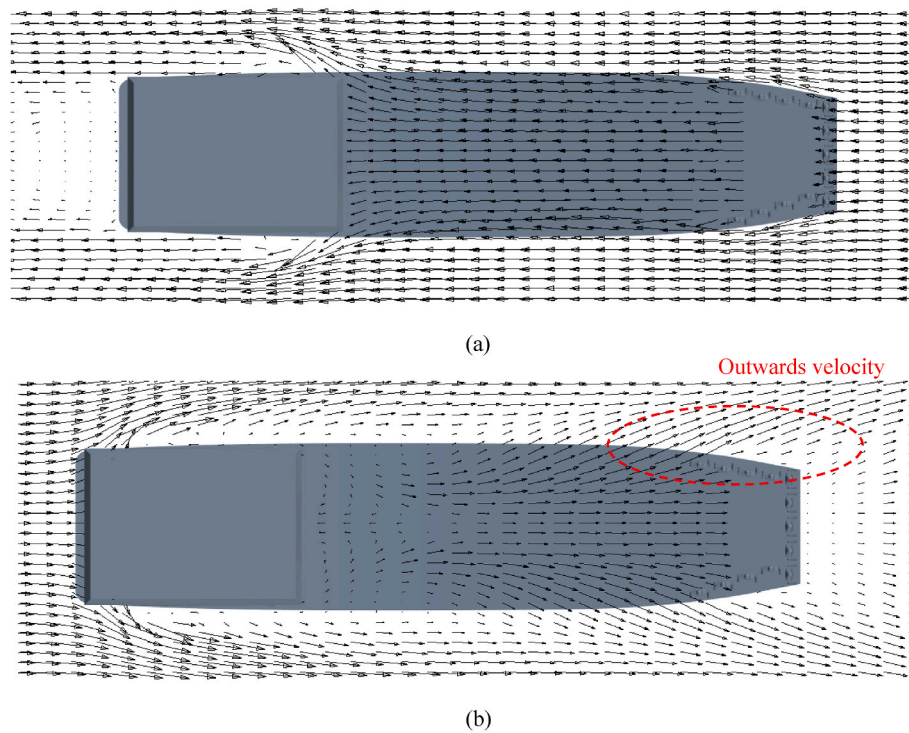


Fig. 13. Comparison of the flow direction under the influence of ship superstructure, between headwind and tailwind: (a) headwind, (b) tailwind.

2.4. Discretisation

In order to solve the governing equations, the computational domain was discretised using the Finite Volume Method (Versteeg and Malalasekera, 2007), with grided domain presented in Fig. 7. The computational domain was discretised into a mesh using hexahedral cells. The cell shape is based on cubic while the shape may change in particular regions, e.g. due to the curvature of the hull. An overset mesh was applied around the ship to enable ship motions (Huang et al., 2022b). To obtain high-resolution results for the fluid flows surrounding the ship

and the associated virus movements, a refined grid size was used for the overset mesh ($d = \Delta x = \Delta y = \Delta z$) and for the free surface region ($d = \Delta z$), whereas a relatively large grid size ($10d$) was applied for regions that are relatively far from the ship. When the particulate flow is simulated following the present computational approach, the number of particles inside per cell may be obtained.

To justify the rationality of the present model, a Validation and Verification (V&V) process has been conducted. Firstly, the computational method including the governing equations, virus treatment, and the Euler–Lagrange coupling was used to replicate an experimental case

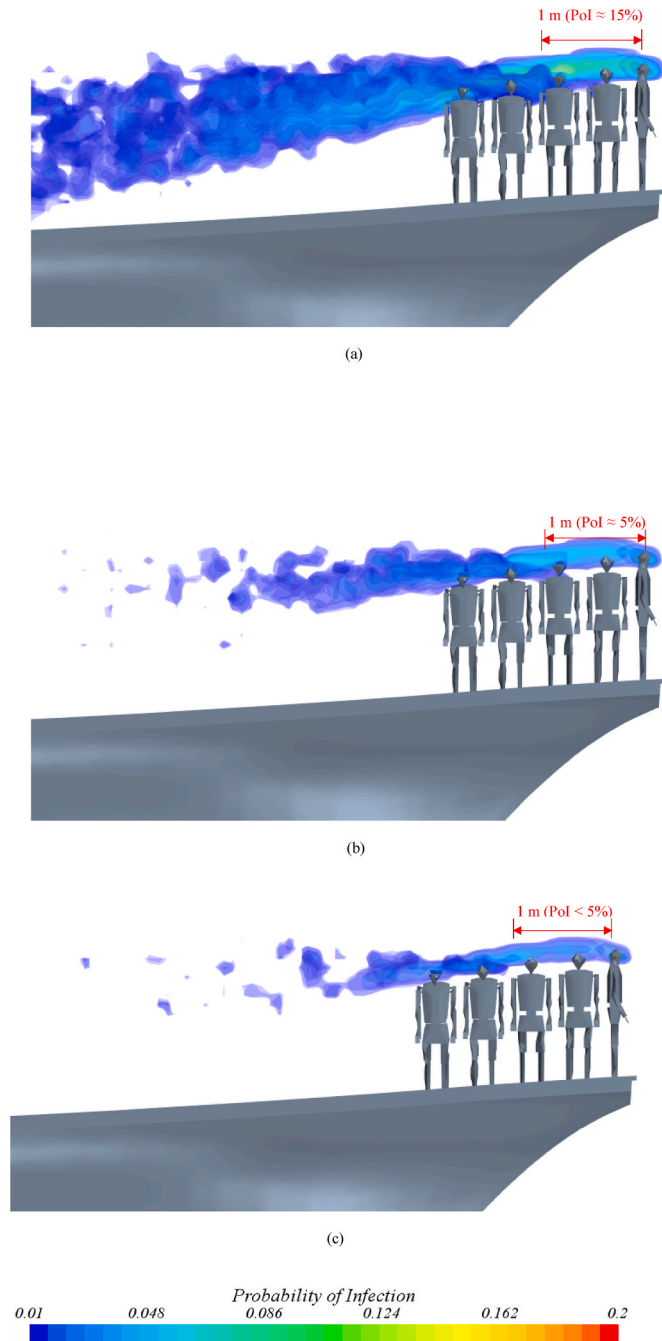


Fig. 14. Comparison of PoI with different wind speeds, considering an infected person speaking for 20 min, $\theta = 0^\circ$: (a) $V = 1$ m/s, (b) $V = 3$ m/s, (c) $V = 5$ m/s.

of particulate flow in a cuboid chamber, as reported in Huang et al. (2022a). Upon validating the method, verification was conducted by analysing the mesh sensitivity of the present fishing vessel case, introduced as follows.

As the computational cost increases with increasing the cell number, a mesh sensitivity study was conducted in order to get a reliable solution using as few cells as possible. Since the fluid flow is Eulerian and virus particles are Lagrangian, only the fluid part is grided. Therefore, the fluid flow around the ship was examined using three different mesh densities, as $d_1 = 0.15$ m, $d_2 = 0.11$ m, $d_3 = 0.08$ m, corresponding to a total cell number of 3.3, 8.0, and 20.8 million, namely Coarse, Fine, and Very Fine meshes, respectively. The three sets of mesh were examined using a test case of $V = 2$ m/s and $\theta = 0^\circ$.

The size of each timestep was determined by a prescribed Courant

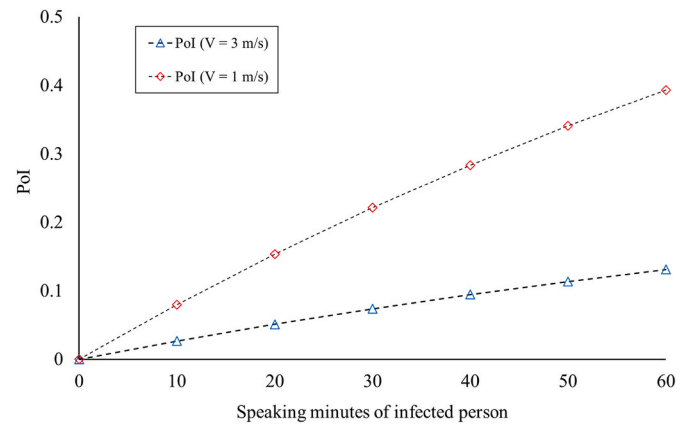


Fig. 15. Infection risk for healthy passengers within a 1 m wake of the infected person in headwind condition, as a function of the speaking time of the infected person, $\theta = 0^\circ$.

number (Co) value, according to the expression in Equation (10):

$$Co = \frac{v_n \Delta t}{d} \tag{10}$$

where Δt denotes the time step size, v_n is the flux speed through the shared face between two neighbouring cells, and Δx is its distance between the centres of two cells. The max Co value is set at 1 which is standard practice (ITTC, 2014). Based on this index, the timestep size is automatically varied according to the tested cell size.

The results of the mesh sensitivity study are checked by making quantitative comparison between the Coarse, Fine and Very Fine meshes. As shown in Fig. 8, three significant locations in the air/particle flow were selected to extract data. The velocity magnitude and particle concentration of the three points were compared between the meshes, as plotted in Fig. 9. It can be seen that the results converge with increasing cell number, while the improvement between Fine and Very Fine meshes is not tangible. Therefore, the Fine mesh set was selected to perform the simulations.

3. Results and discussion

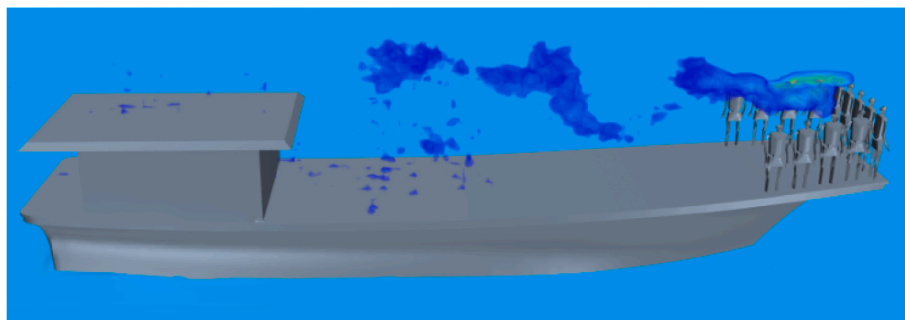
3.1. Virus distribution at different wind speeds and directions

When the ship is subjected to airflow and a person onboard disseminates the virus, the particles follow the movement of the wind and form a wake behind the person. Along the wake, the virus particles diffuse and become widely dispersed after travelling a certain distance. Considering an infected person injecting virus particles at a constant speed, with a uniform airflow, ngth, shape, and virus distribution. The virus distribution does not vary notably between transient solutions, thus an instantaneous time may be used to present the results. The virus wakes in different speeds of headwinds are shown in Figs. 10 and 11. It can be seen that the crew situated downstream of the infected person may be surrounded by high-concentration viruses, thus they are vulnerable to infection. The figures show that both the virus coverage and concentration reduce with increasing wind speed. This indicates that the virus diffuses quicker when the wind speed is stronger, thereby reducing the risk of COVID-19 transmission among crew. Moreover, the forward door and windows of the superstructure may be kept closed in a headwind condition to prevent the virus from entering the cabin, and it is recommended to regularly clean these areas.

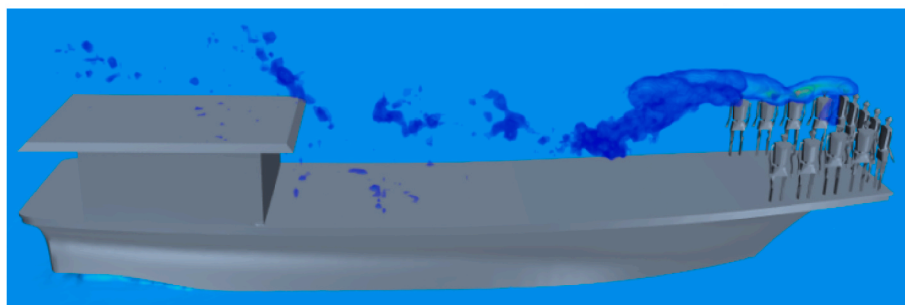
The virus distributions with different wind directions are compared and presented in Fig. 12, presenting for the airflow speed of $V = 1$ m/s as this shows the greatest risk among the five studied speeds. The virus distribution behaves similarly when $\theta = 0^\circ - 135^\circ$, but when $\theta = 180^\circ$, the virus is directed outward of the ship and the downstream crew has the

Table 3
Motions of the vessel in a representative set of sea conditions, $T = 10$ s and $H = 2$ m.

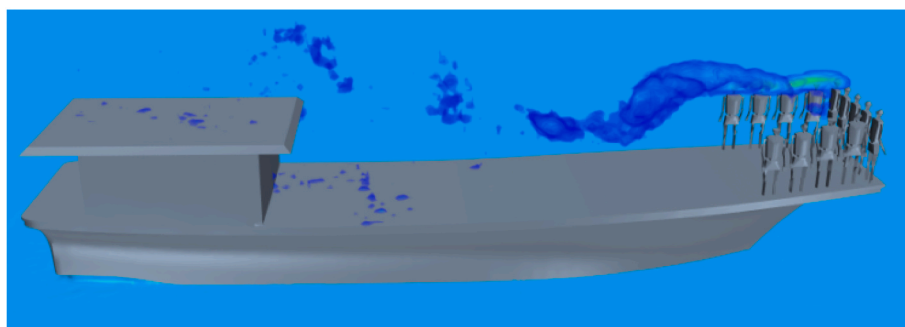
	Heave amplitude	Heave period	Pitch amplitude	Pitch period	Roll amplitude	Roll period
Head Sea	0.968 m	13.7 s	6.18°	13.7 s	N/A	N/A
Beam Sea	0.884 m	8.9 s	N/A	N/A	11.24°	5.9 s
Following Sea	1 m	6 s	3.24°	3.7 s	N/A	N/A



(a)



(b)



(c)

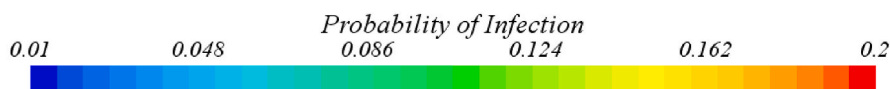


Fig. 16. Transmission of the virus coupled with ship motions in head seas, considering an infected person speaking for 20 min: (a) $t = nT$, (b) $t = nT + 1/2T$, (c) $t = (n+1)T$.

smallest risk in this scenario. This is because the ship’s superstructure can scatter the airflow, diverting it outward.

A clear comparison of the flow direction is given in Fig. 13. If the ship is not moving, placing the stern in the direction of the wind could reduce the spread of COVID-19. Nonetheless, as the ship is often moving, the actual airflow may still be a headwind due to the relative motion. The ship superstructure cannot be used to divert the particulate flow in such

situations and a COVID-19 risk assessment is still essential.

3.2. Risk assessment

Based on the results from the model, a person’s mouth can be immersed in a flow with a certain concentration of virus. The average air intake per person for moderate physical activities like fishing is $1.4 \text{ m}^3/\text{h}$

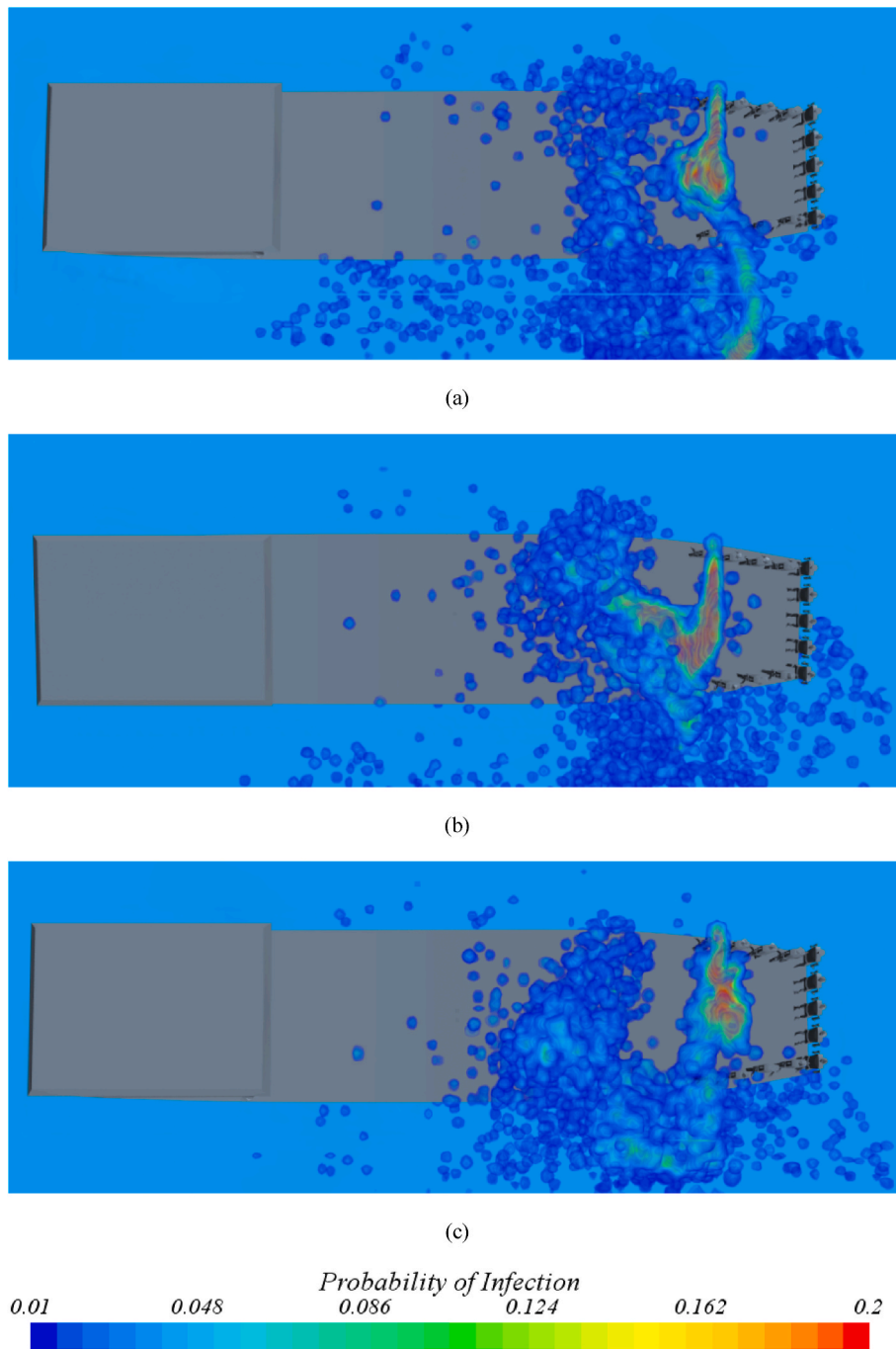


Fig. 17. Transmission of the virus coupled with ship motions in beam seas, considering an infected person speaking for 20 min: (a) $t = nT$, (b) $t = nT + 1/2T$, (c) $t = (n+1)T$.

(U.S.E.P.A.O. of Health E.A.E.A. Group, 1989). Over a certain duration of time, the total inhalable virus number (N) at a location can be calculated based on the virus concentration. To estimate the COVID-19 risk level in this scenario, the Probability of Infection (PoI) can be calculated using Equation (11) (Ando et al., 2022; Bale et al., 2022):

$$PoI = 1 - e^{-\frac{N}{N_0}} \quad (11)$$

where N_0 is the number of inhaled virus particles needed for COVID-19 infection. The exact value of N_0 varies on a scenario, while an approximate value can be obtained based on past COVID-19 events (Vuorinen et al., 2020; Shen et al., 2020; Luo et al., 2020; Jang et al., 2020; Park et al., 2020; Hamner, 2020). Prentiss et al. (2020) analysed a series of

events and suggested that the minimal number of N_0 is 300. According to Equation (11), the higher N_0 will lower the PoI, thus this work adopts the minimal number of N_0 of 300 so that the risk in the present case is not underestimated.

The corresponding PoI results are shown in Fig. 14, where the PoI within 1 m wake is an average of $\sim 15\%$ for $V = 1$ m/s and $\sim 5\%$ for $V = 3$ m/s. The risks of different cases are assessed based on the same period of time, considering an infected person speaking for 20 min. When the infected person's speaking time is varied, the imported virus number will change, and so will the risk level; the PoI of different speaking times is given in Fig. 15, which demonstrates a clear benefit from reducing talking. Overall, it can be seen that increasing V can reduce the risk to a minimal level. When a ship has a relative speed of higher than 3 m/s to

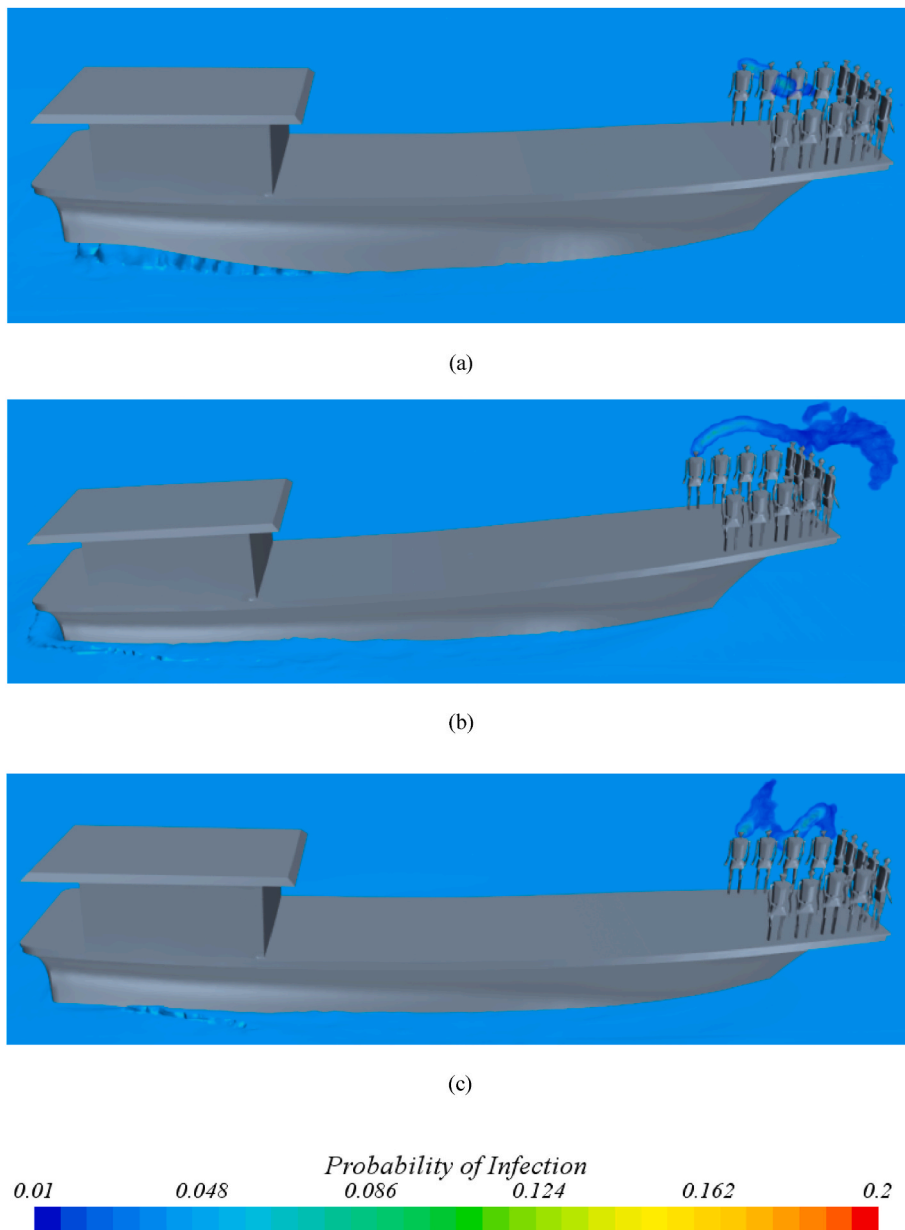


Fig. 18. Transmission of the virus coupled with ship motions in following seas, considering an infected person speaking for 20 min: (a) $t = nT$, (b) $t = nT + 1/2T$, (c) $t = (n+1)T$.

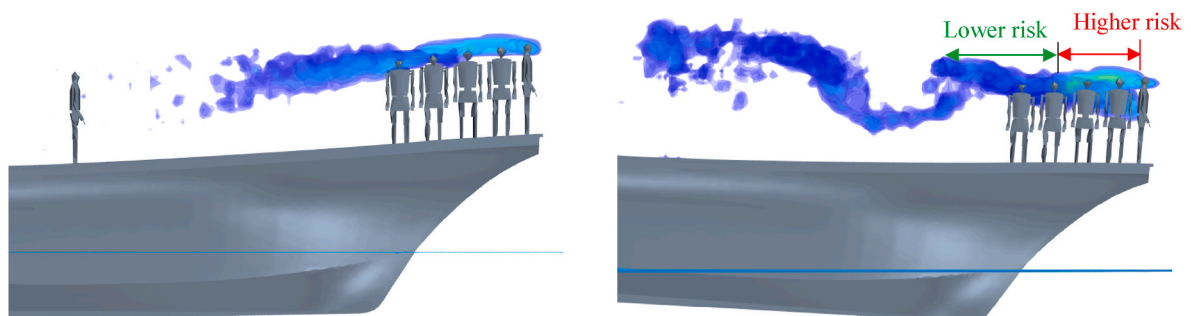


Fig. 19. Comparison of virus transmission without (Left Panel) and with (Right Panel) motions in head seas.

the airflow, the COVID-19 risk on deck is small, even if a person speaks for an extended period. Therefore, it is recommended to control a ship's power to ensure a relative speed of higher than 3 m/s.

3.3. The influence of ship motions

To investigate the virus transmission when the vessel is in motion,

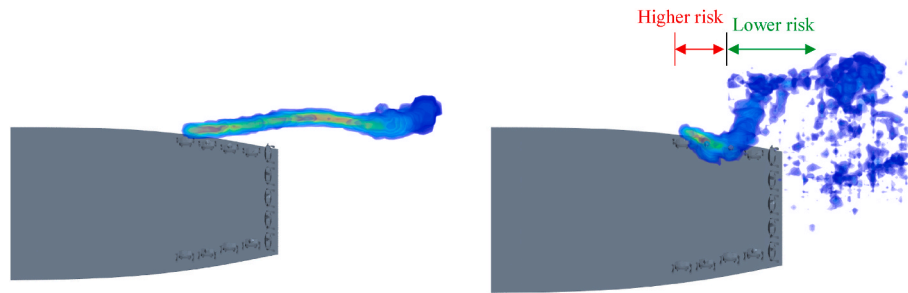


Fig. 20. Comparison of virus transmission without (Left Panel) and with (Right Panel) motions in following seas.

field measurements of the study vessel were conducted, with a representative wave condition selected and analysed with wave period $T = 10$ s and wave height $H = 2$ m. Considering this wave condition from head sea ($\theta = 0^\circ$), beam sea ($\theta = 90^\circ$), and following sea ($\theta = 180^\circ$) directions, the corresponding ship motions were extracted and given in Table 3, using the Maxsurf software. The Maxsurf software first uses the conformal mapping technique to project a ship geometry in the free surface flow, and then the Strip Theory is used to calculate the vessel's added mass, damping and cross-coupling terms, based on which the coupled heave, pitch and rolls motions of a particular vessel in a particular wave condition can be predicted (Xing-yu et al., 2020). These calculated motion amplitudes from Maxsurf were then used to prescribe the ship's motions in the CFD model, using the overset approach (Huang et al., 2022b). Specifically, rigid bodies inside the overset region (Fig. 7) are controlled to conduct 6-DOF motions over time. Thus, the corresponding virus transmission is coupled with the motions, as presented in Figs. 16–18. The advantage of applying this overset prescribing motion approach is to save a substantial computational cost of simulating the full wave hydrodynamics that is not the study object of this work, whilst equivalently modelling the virus transmission coupled with ship motions.

In Fig. 17, It can be seen that the vessel's motions significantly change the trace of the virus particles in beam sea conditions. The roll motion causes the particles to concentrate in the deck region due to the oscillating motions, exposing a wider spread than the calm water scenario. This phenomenon results in the overall risk being much higher than the scenario without roll motions. Therefore, positioning a ship under a beam sea condition should be avoided to minimise the probability of other fishers contracting the virus. When the avoidance of this condition is not possible, the fishers should be alerted and relevant work on deck should be restricted.

In head and following sea conditions, the particle trace becomes a sine-like shape following the ship's motion functions. The following sea condition poses smaller risks than the head seas condition, which matches the results without motions. A detailed comparison is presented in Figs. 19 and 20. It is found the oscillating motions also strengthen the virus concentration in a short distance, while the risk in the wake of a long distance is lower. The length of the higher-risk zone in sea conditions is likely to link with the vessel's motion amplitude - the higher the motion amplitude, the longer the high-risk zone. It can be seen that the higher-risk zone in following seas is shorter than that in head seas, as the pitch amplitude in following seas is smaller. Moreover, in following seas condition, the bluff body effect (Fig. 13) of the superstructure is no longer evident due to the ship movement, as shown in Fig. 20.

4. Conclusions

To investigate the COVID-19 risk and mitigation efforts required in offshore environments, a computational model has been developed to investigate the airborne coronavirus transmission around the deck of an Indonesian PL fishing vessel. Based on the model, a variety of typical scenarios were simulated, including different wind directions, wind

speeds and ship motions in different waves. In particular, a risk assessment index, i.e. PoI, was implemented to provide a quantitative understanding of spreading events.

It was demonstrated that the virus transmission generally follows the airflow direction that a ship is subjected to, and the virus concentration diffuses in a wake form. A higher wind speed facilitates the virus diffusion, thus lowering the COVID-19 risk. Whilst a significant COVID-19 risk emerges in low wind speed conditions, the ship's superstructure was observed to divert the wind flow which drives the virus particles away from the ship. Therefore, it is recommended to position the ship's stern into the wind when and where possible.

Subsequently, this research highlighted that the virus transmission trace significantly changes with ship motions. Compared to the calm water scenarios, the risk level increased within a short wake but decreased in a comparatively long distance. This is because the ship's oscillating movement in waves can reinforce the virus concentration in close proximity to the infected person, and in the farther part of the wake, the motions help diffuse the virus. This proximity distance was shown to create a particularly high-risk profile for a ship in beam seas, which is linked to the beam dimension being a fraction of the ship's length dimension.

Overall, the present study identified a series of high-risk and low-risk scenarios for the combined wind and wave conditions, together with their underlying physical mechanisms. The presented modelling approach and findings provide insights to help offshore and maritime stakeholders to better understand and assess the COVID-19 spreading risks during operations. This will further lead to scenario-based precautions and protective measures, as well as being useful if a similar airborne transmission disease outbreaks offshore and the crew need to quickly adopt configurations to minimise the virus spread.

In addition, it is noted that social distancing was not discussed in this paper, except for the general rule that staying farther from each other will reduce the infection risk. This is because social distancing is hard to implement for the PL fishing scenario due to the need to throw baits at concentrated locations to improve efficiency. In practice, the fishermen stay close to each other despite potential operational difficulties such as the possibility to have tangled fishing lines.

CRedit authorship contribution statement

Luofeng Huang: Conceptualization, Data curation, Formal analysis, Investigation, Methodology, Resources, Software, Visualization, Writing – original draft. **Volter Hetharia:** Conceptualization, Data curation, Investigation, Resources, Visualization. **Andrea Grech La Rosa:** Investigation, Project administration, Writing – review & editing. **Sasan Tavakoli:** Conceptualization, Methodology, Writing – review & editing. **Danial Khojasteh:** Formal analysis, Visualization, Writing – review & editing. **Minghao Li:** Methodology, Software, Visualization. **Soengeng Riyadi:** Data curation, Investigation. **Dony Setyawan:** Investigation, Project administration. **I.K.A.P. Utama:** Funding acquisition, Investigation, Project administration, Resources. **Giles Thomas:** Conceptualization, Funding acquisition, Project administration, Resources,

Supervision, Writing – review & editing.

Declaration of competing interest

The authors declare that they have no known competing financial interests or personal relationships that could have appeared to influence the work reported in this paper.

Data availability

All data underlying the results are available as part of the article and no additional source data are required.

Acknowledgements

This work has been supported by funding from the British Council under the Newton Institutional Links Grants – Project Title: Ensuring the safety of Indonesian seafarers and fishers in the time of COVID-19 and beyond (agreement No. 623457938). The Indonesian authors appreciate financial support from the Indonesian Ministry of Education (agreement No. 1369/PKS/TTS/2022). The CV Yora fishing company is thanked for sharing the details of the studied vessel.

References

- Abuhegazy, M., Talaat, K., Anderoglu, O., Poroseva, S.V., 2020. Numerical investigation of aerosol transport in a classroom with relevance to COVID-19. *Phys. Fluids* 32, 103311.
- Adzic, F., Roberts, B.M., Hathway, E.A., Matharu, R.K., Ciric, L., Wild, O., Cook, M., Malki-Epstein, L., 2022. A post-occupancy study of ventilation effectiveness from high-resolution CO₂ monitoring at live theatre events to mitigate airborne transmission of SARS-CoV-2. *Build. Environ.* 223, 109392.
- Almilaji, O., 2021. Air recirculation role in the spread of COVID-19 onboard the diamond princess cruise ship during a quarantine period. *Aerosol Air Qual. Res.* 21, 200495.
- Ando, K., Bale, R., Li, C., Matsuoka, S., Onishi, K., Tsubokura, M., 2022. Digital transformation of droplet/aerosol infection risk assessment realized on “Fugaku” for the fight against COVID-19. *Int. J. High Perform. Comput. Appl.* 36, 568–586.
- Azimi, P., Keshavarz, Z., Cedeno Laurent, J.G., Stephens, B., Allen, J.G., 2021. Mechanistic transmission modeling of COVID-19 on the Diamond Princess cruise ship demonstrates the importance of aerosol transmission. *Proc. Natl. Acad. Sci. USA* 118, e2015482118.
- Bale, R., Iida, A., Yamakawa, M., Li, C., Tsubokura, M., 2022. Quantifying the COVID-19 infection risk due to droplet/aerosol inhalation. *Sci. Rep.* 12, 11186.
- Chao, C.Y.H., Wan, M.P., Morawska, L., Johnson, G.R., Ristovski, Z.D., Hargreaves, M., Mengersen, K., Corbett, S., Li, Y., Xie, X., 2009. Characterization of expiration air jets and droplet size distributions immediately at the mouth opening. *J. Aerosol Sci.* 40, 122–133.
- Chua, J.Y., Foo, R., Tan, K.H., Yuen, K.F., 2022. Maritime Resilience during the COVID-19 Pandemic: Impacts and Solutions, Continuity & Resilience Review.
- D’Antoine, E., Jansz, J., Barifcani, A., Shaw-Mills, S., Harris, M., Lagat, C., 2023. COVID-19 and Offshore Oil and Gas Workers: the Role of Personality. *Social Sciences & Humanities Open*, 100402.
- Gosman, A.D., Ioannides, E., 1983. Aspects of computer simulation of liquid-fueled combustors. *J. Energy* 7, 482–490.
- Hammer, L., 2020. High SARS-CoV-2 Attack Rate Following Exposure at a Choir Practice—Skagit County, Washington, March 2020, MMWR. Morbidity and Mortality Weekly Report, 69.
- Hirt, C.W., Nichols, B.D., 1981. Volume of fluid (VOF) method for the dynamics of free boundaries. *J. Comput. Phys.* 39, 201–225.
- Huang, L., Tuhkuri, J., Igrec, B., Li, M., Stagonas, D., Toffoli, A., Cardiff, P., Thomas, G., 2020. Ship resistance when operating in floating ice floes: a combined CFD&DEM approach. *Mar. Struct.* 74, 102817.
- Huang, L., Riyadi, S., Utama, I., Li, M., Sun, P., Thomas, G., 2022a. COVID-19 transmission inside a small passenger vessel: risks and mitigation. *Ocean. Eng.* 255, 111486 <https://doi.org/10.1016/j.oceaneng.2022.111486>.
- Huang, L., Li, F., Li, M., Khojasteh, D., Luo, Z., Kujala, P., 2022b. An investigation on the speed dependence of ice resistance using an advanced CFD+ DEM approach based on pre-sawn ice tests. *Ocean. Eng.* 264, 112530.
- Huang, L., Pena, B., Thomas, G., 2023. Towards a Full-Scale CFD Guideline for Simulating a Ship Advancing in Open Water. *Ship Technology Research*, pp. 1–17. ITTC, 2014. Guidelines: Practical Guidelines for Ship CFD Applications. ITTC Report.
- Jang, S., Han, S.H., Rhee, J.-Y., 2020. Cluster of coronavirus disease associated with fitness dance classes, South Korea. *Emerg. Infect. Dis.* 26, 1917.
- Janoszek, T., Lubosik, Z., Świerczek, L., Walentek, A., Jaroszewicz, J., 2021. Experimental and CFD simulations of the aerosol flow in the air ventilating the underground excavation in terms of SARS-CoV-2 transmission. *Energies* 14, 4743. <https://doi.org/10.3390/en14164743>.
- Jeong, D., Yi, H., Park, J.-H., Park, H.W., Park, K., 2022. A vertical laminar airflow system to prevent aerosol transmission of SARS-CoV-2 in building space: computational fluid dynamics (CFD) and experimental approach. *Indoor Built Environ.* 31, 1319–1338. <https://doi.org/10.1177/1420326X211063422>.
- Khojasteh, D., Davani, E., Shamsipour, A., Haghani, M., Glamore, W., 2022. Climate change and COVID-19: interdisciplinary perspectives from two global crises. *Sci. Total Environ.* 844, 157142.
- Liu, A.B., Mather, D., Reitz, R.D., 1993. Modeling the effects of drop drag and breakup on fuel sprays. *SAE Trans.* 83–95.
- Luo, K., Lei, Z., Hai, Z., Xiao, S., Rui, J., Yang, H., Jing, X., Wang, H., Xie, Z., Luo, P., 2020. Transmission of SARS-CoV-2 in public transportation vehicles: a case study in Hunan Province, China. In: *Open Forum Infectious Diseases*. Oxford University Press US, p. ofaa430.
- Menter, F., 1993. Zonal two equation kw turbulence models for aerodynamic flows. In: *23rd Fluid Dynamics, Plasmadynamics, and Lasers Conference*, p. 2906.
- Mohamadi, F., Fazeli, A., 2022. A review on applications of CFD modeling in COVID-19 pandemic. *Arch. Comput. Methods Eng.* 29, 3567–3586.
- Moritz, S., Gottschick, C., Horn, J., Popp, M., Langer, S., Klee, B., Purschke, O., Gekle, M., Ihling, A., Zimmermann, F.D., 2021. The risk of indoor sports and culture events for the transmission of COVID-19. *Nat. Commun.* 12, 5096.
- Park, S.Y., Kim, Y.-M., Yi, S., Lee, S., Na, B.-J., Kim, C.B., Kim, J., Kim, H.S., Kim, Y.B., Park, Y., 2020. Coronavirus disease outbreak in call center, South Korea. *Emerg. Infect. Dis.* 26, 1666.
- Pena, B., Huang, L., 2021. A review on the turbulence modelling strategy for ship hydrodynamic simulations. *Ocean. Eng.* 241, 110082.
- Prentiss, M., Chu, A., Berggren, K.K., 2020. Superspreading events without superspreaders: using high attack rate events to estimate N⁰ for airborne transmission of COVID-19. *medRxiv*, 2020–10.
- Sarhan, A.R., Naser, P., Naser, J., 2021. COVID-19 aerodynamic evaluation of social distancing in indoor environments, a numerical study. *J. Environ. Health Sci. Eng.* 19, 1969–1978.
- Shen, Y., Li, C., Dong, H., Wang, Z., Martinez, L., Sun, Z., Handel, A., Chen, Z., Chen, E., Ebell, M.H., 2020. Community outbreak investigation of SARS-CoV-2 transmission among bus riders in eastern China. *JAMA Intern. Med.* 180, 1665–1671.
- Talaat, K., Abuhegazy, M., Mahfoze, O.A., Anderoglu, O., Poroseva, S.V., 2021. Simulation of aerosol transmission on a Boeing 737 airplane with intervention measures for COVID-19 mitigation. *Phys. Fluids* 33, 033312.
- Tavakoli, S., Khojasteh, D., Haghani, M., Hirdaris, S., 2023. A review on the progress and research directions of ocean engineering. *Ocean. Eng.* 272, 113617.
- Thanigaiarasu, S., Balamani, G., Bakiya, A., Immaculyne, F., Kamalanand, K., De Britto, R.L.J., 2022. Numerical modeling and simulation of the droplet transmission of SARS-CoV-2 in the ambient environment and its relevance to social distancing. *Math. Probl. Eng.* 1–10, 2022.
- Thomas, G., Huang, L., Ryan, C., Utama, I., Riyadi, S., Setyawan, D., Hetharia, W., 2021. Safer onboard environments for Indonesian seafarers and Fishers in the time of COVID-19 and beyond. In: *International Conference on Ship and Offshore Technology*. The Royal Institution of Naval Architects (RINA), Surabaya, Indonesia.
- Tu, Q., Mo, J., Liu, Z., Gong, C., Fan, Y., 2021. Using green finance to counteract the adverse effects of COVID-19 pandemic on renewable energy investment-The case of offshore wind power in China. *Energy Pol.* 158, 112542.
- U.S.E.P.A.O. of Health, E.A.E.A. Group, 1989. *Exposure Factors Handbook*. Office of Health and Environmental Assessment, US Environmental Protection Agency.
- Versteeg, H.K., Malalasekera, W., 2007. *An Introduction to Computational Fluid Dynamics: the Finite Volume Method*. Pearson Education.
- Vuorinen, V., Aarnio, M., Alava, M., Alopaeus, V., Atanasova, N., Auvinen, M., Balasubramanian, N., Bordbar, H., Erästö, P., Grande, R., 2020. Modelling aerosol transport and virus exposure with numerical simulations in relation to SARS-CoV-2 transmission by inhalation indoors. *Saf. Sci.* 130, 104866.
- Wang, C.C., Prather, K.A., Sznitman, J., Jimenez, J.L., Lakdawala, S.S., Tufekci, Z., Marr, L.C., 2021. Airborne transmission of respiratory viruses. *Science* 373, eabd9149.
- Wang, Z., Galea, E.R., Grandison, A., Ewer, J., Jia, F., 2022. A coupled Computational Fluid Dynamics and Wells-Riley model to predict COVID-19 infection probability for passengers on long-distance trains. *Saf. Sci.* 147, 105572.
- Wibawa, I.P.A., Birmingham, R., 2018. Improving safety working environment on Indonesian fishing fleet: a case study on local fishing communities in East Java. In: *Maritime Safety International Conference (MASTIC 2018)*. Newcastle University.
- Xing-yu, L., Yan-ping, H., Chao, C., 2020. Analysis of the seakeeping performance of icebreaker based on Maxsurf. In: *The 30th International Ocean and Polar Engineering Conference*. OnePetro.
- Zhang, Z., Han, T., Yoo, K.H., Capecehatro, J., Boehman, A.L., Maki, K., 2021. Disease transmission through expiratory aerosols on an urban bus. *Phys. Fluids* 33, 015116.
- Zhang, M., Shrestha, P., Liu, X., Turmagoğlu, T., DeGraw, J., Schafer, D., Love, N., 2022. Computational fluid dynamics simulation of SARS-CoV-2 aerosol dispersion inside a grocery store. *Build. Environ.* 209, 108652.
- Zhao, L., Zou, Y., Li, Y., Miyani, B., Spooner, M., Gentry, Z., Jacobi, S., David, R.E., Withington, S., McFarlane, S., 2022. Five-week warning of COVID-19 peaks prior to the Omicron surge in Detroit, Michigan using wastewater surveillance. *Sci. Total Environ.* 844, 157040.